Neuron, Vol. 26, 55–67, April, 2000, Copyright ©2000 by Cell Press

Dynamic Statistical Parametric Neurotechnique Mapping: Combining fMRI and MEG for High-Resolution Imaging of Cortical Activity

Anders M. Dale,*‖ Arthur K. Liu,* Bruce R. Fischl,* Randy L. Buckner,§ John W. Belliveau,* Jeffrey D. Lewine,† and Eric Halgren*†‡

*Massachusetts General Hospital Nuclear Magnetic Resonance Center
Charlestown, Massachusetts 02129
†Department of Radiology
University of Utah
Salt Lake City, Utah 84108
‡Institut National de la Santé et de la Recherche Médicale
E9926, Marseilles
France
§Department of Psychology Anatomy, and Neurobiology, and Radiology
Washington University
St. Louis, Missouri 63130

Summary

Functional magnetic resonance imaging (fMRI) can provide maps of brain activation with millimeter spatial resolution but is limited in its temporal resolution to the order of seconds. Here, we describe a technique that combines structural and functional MRI with magnetoencephalography (MEG) to obtain spatiotemporal maps of human brain activity with millisecond temporal resolution. This new technique was used to obtain dynamic statistical parametric maps of cortical activity during semantic processing of visually presented words. An initial wave of activity was found to spread rapidly from occipital visual cortex to temporal, parietal, and frontal areas within 185 ms, with a high degree of temporal overlap between different areas. Repetition effects were observed in many of the same areas following this initial wave of activation, providing evidence for the involvement of feedback mechanisms in repetition priming.

Introduction

Thorough understanding of the functional organization of the brain requires knowledge of several aspects of functional neuroanatomy, including the specific locations of processing areas, the type of processing performed, the time course of processing, and the nature of the interactions between these areas. Local alterations in neuronal activity induce local changes in the electric and magnetic fields (Hämäläinen et al., 1993; Mitzdorf, 1985), cerebral metabolism, and cerebral perfusion (blood flow, blood volume, and blood oxygenation) (Mazziotta et al., 1983; Fox and Raichle, 1986; Fox et al., 1988; Belliveau et al., 1991; Prichard et al., 1991; Kwong et al., 1992). Several noninvasive techniques exist that measure changes in these hemodynamic and electromagnetic signals. Considered individually, these techniques offer trade-offs between spatial and temporal resolution (Churchland and Sejnowski, 1988). Hemodynamic assessment of brain activity is temporally limited by the latency of the hemodynamic response (about 1 s) but can provide millimeter spatial sampling (Belliveau et al., 1991; Kwong et al., 1992). Conversely, methods based on direct measurement of the electric and magnetic fields produced by neuronal activity can provide temporal resolution of less than 1 ms, adequate for detecting the orchestration of complex cognitive activity (Regan, 1989). However, the *spatial* configuration of neuronal activity cannot be derived uniquely based on electroencephalography (EEG) and/or magnetoencephalography (MEG) recordings alone (Nunez, 1981; Hämäläinen et al., 1993). In order to make this so-called *inverse problem* well posed, it is necessary to impose additional constraints on the solution.

One common approach is to assume that the EEG/MEG signals are generated by a relatively small number of focal sources (Sherg and VonCramon, 1985; Schmidt et al., 1999). An additional constraint can be derived from the assumption that the sources are temporally uncorrelated (Mosher et al., 1992). These assumptions are particularly appropriate when analyzing early sensory responses, where the activity might reasonably be expected to be relatively focal and constrained to a few primary sensory areas. On the other hand, such assumptions are less justified in higher-level cognitive experiments, which have been found by intracranial recordings in humans to involve extensive networks of more or less synchronously activated brain areas (Halgren et al., 1994a, 1994b, 1995a, 1995b; Baudena et al., 1995). Similarly, the interictal spikes characteristic of partial epilepsy typically spread very rapidly to involve a network extended across multiple cortical and limbic regions (Chauvel et al., 1987).

An alternative approach to analyzing EEG/MEG signals is to impose constraints based on anatomical and physiological information derived from other imaging modalities. The anatomical constraint is based on the observation that the main cortical generators of EEG and MEG signals are localized to the gray matter and oriented perpendicularly to the cortical sheet (Nunez, 1981). Thus, once the exact shape of the cortical surface is known (for a specific subject), this information can be used to greatly reduce the EEG/MEG solution space (Dale and Sereno, 1993).

The solution space can be further reduced by making use of information derived from metabolic or hemodynamic measures of brain activity during the same task (Nenov et al., 1991; Dale and Sereno, 1993; Heinze et al., 1994; Snyder et al., 1995; Liu et al., 1998; Mangun et al., 1998; Ahlfors et al., 1999). This is based on the hypothesis that the synaptic currents generating the EEG/MEG signals also impose metabolic demands, which in turn lead to a hemodynamic response measurable using positron emission tomography (PET) (Raichle,

‖To whom correspondence should be addressed (e-mail: dale@nmr.mgh.harvard.edu).

1987) or functional magnetic resonance imaging (fMRI) (Belliveau et al., 1991; Kwong et al., 1992). Although the precise nature of the coupling between neuronal activity and hemodynamic signals is unknown, there is considerable evidence for a strong correlation between the spatial patterns of hemodynamic changes and neuronal electrical activity over time in both animals (Grinvald et al., 1986) and humans (Benson et al., 1996; Puce et al., 1997).

Here we present a general framework for integrating information from different imaging modalities with a priori anatomical and physiological information to produce spatiotemporal estimates of brain activity. By normalizing these estimates in terms of noise sensitivity at each spatial location, we obtain statistical parametric maps (SPMs) that provide information about the statistical reliability of the estimated signal at each location in the map with millisecond accuracy. These SPMs can then be visualized as movies of brain activity (dynamic SPMs). In order to quantitate the spatial resolution of these maps, we compute the pointspread function for different locations on the cortical surface. This reflects the spatial "blurring" of the true activity patterns in our spatiotemporal maps or movies.

This new method is applied to MEG and fMRI measurements in a task involving semantic judgments of visually presented words. Such tasks are known to involve a large number of cortical areas (Buckner and Koutstaal, 1998; Fiez and Petersen, 1998), but the timing of their involvement has not previously been determined. The putative roles assigned to these structures suggest a possible sequence of activation during this task, with visual word form processing preceding semantic associative activation, which in turn would precede working memory and response mapping. It is unknown if, in fact, processing occurs according to this sequence. More generally, the degree to which processing is sequential and modular in specialized regions versus parallel and distributed is unknown.

In addition, we investigated the effect of item repetition on the spatiotemporal activity patterns evoked by the task. Repetition is also known to alter the activation evoked in several cortical regions (Buckner and Koutstaal, 1998; Gabrieli et al., 1998), but again, the timing of these effects is not known. One hypothesis would suggest that processing of repeated items is facilitated beginning with relatively early perceptual stages. An alternative hypothesis is that repetition effects are mediated by a top-down mechanism, originating in higher-level brain areas. One way to distinguish between these hypotheses would be to know the order in which different anatomical areas show the effects of repetition. The area with the earliest changes might then be reasonably supposed to help produce the later changes noted in other areas. Note that an observed decrease in metabolism in cortical areas that are "early" in the anatomical sense (e.g., sensory-perceptual areas) might nonetheless be due to a change that occurs late in time (i.e., late in the processing stream) due to top-down effects from higher areas. Thus, the actual timing, as well as the location of activation, is crucial for understanding the functional dynamics of cognitive processing.

Results and Discussion

Estimation of Spatiotemporal Activity Patterns

The goal of the method described here is to obtain estimates of brain electrical activity with the best possible spatial and temporal accuracy. Given the inherent differences in the spatial and temporal resolution of noninvasive imaging modalities, as discussed above, we wish to combine the different measures in a way that takes maximal advantage of the strengths of each technique. In other words, we wish to obtain spatiotemporal activity estimates that are maximally consistent with all available observables (i.e., fMRI, EEG, and/or MEG) as well as a priori anatomical and physiological information (for a more formal discussion, see Experimental Procedures below, and Liu, 2000). This, of course, requires that we have some idea of the coupling between electrical activity in the brain and our noninvasive observables. In the case of EEG and MEG, this is relatively straightforward, as the electric and magnetic fields generated by neuronal activity follows from well understood fundamental laws of physics (Nunez, 1981; Hämäläinen et al., 1993).

The primary generators of EEG and MEG are synaptic currents, where the current flows crossing neuronal membranes act as tiny current sources or sinks for current outflow and inflow, respectively. Note that for each neuron, the net current inflow and outflow through its membrane has to be zero (for conservation of charge). Thus, in order for these fields not to cancel out at the noninvasive sensors, there has to be some net spatial separation between the current sources and sinks within the neurons. Of course, the fields produced by individual neurons are far too weak to be observed noninvasively by EEG or MEG. Thus, to generate externally detectable signals, the neurons within a volume of tissue must be aligned and their synaptic current flows correlated in time. The scalp-recorded EEG and MEG reflect the linear superposition of the fields generated by all such synaptic currents across all neurons.

Of all the neurons in the human brain, the cortical pyramidal cells are particularly well suited to generate externally observable electric and magnetic fields due to their elongated apical dendrites, systematically aligned in a columnar fashion perpendicular to the cortical sheet. Inhibitory and excitatory synaptic inputs from different cell populations have characteristic laminar distributions, resulting in characteristic spatial and temporal patterns of net synaptic current flows at different depths through the cortical sheet (Nicholson and Freeman, 1975; Mitzdorf, 1985; Barth and Di, 1991; Schroeder et al., 1995). These current flows are typically strongly correlated laterally along the cortical sheet (Sukov and Barth, 1998). Since the thickness of the cortical sheet is much smaller than the distance to the EEG and MEG sensors, the current source/sink distribution within a small slab of cortex can be represented by a current dipole oriented perpendicularly to the local cortical surface (Dale and Sereno, 1993), whose strength (moment) varies with time. Thus, we can represent the net cortical synaptic current flows by a scalar function $s(\mathbf{r},t)$, reflecting dipole strength as a function of location $\mathbf{r}$ and time t. The coupling between the dipole strengths and the observed electric and magnetic fields can then be

expressed simply in terms of a sum or integral across all spatial locations (equations 2 and 3 in Experimental Procedures, below).

The coupling between electrical activity and hemodynamic measures like fMRI is less understood. In particular, there is little quantitative data on how the *magnitude* of the hemodynamic response varies as a function of the amplitude and duration of electrical activity. There is, however, considerable evidence for a strong degree of *spatial* correlation between various measures of local electrical activity and local hemodynamic signals. Some of the strongest evidence for this comes from a direct comparison of maps obtained using voltage-sensitive dyes, reflecting depolarization of neuronal membranes in superficial cortical layers, and maps derived from intrinsic optical signals, reflecting changes in light absorption due to changes in blood volume and oxygenation (Shoham et al., 1999). Previous animal studies have also shown strong correlation between local field potentials, spiking activity, and voltage-sensitive dye signals (Arieli et al., 1996; Tsodyks et al., 1999). Furthermore, studies in humans comparing the localization of functional activity using invasive electrical recordings and fMRI also provide evidence of correlation between the local electrophysiological and hemodynamic response (Benson et al., 1996; Puce et al., 1997). This suggests that the local fMRI response can be used to bias the electrical activity estimate toward those regions that show the greatest fMRI response. This can be accomplished by using the fMRI response as an a priori estimate of the locally integrated dipole activity over time (Dale and Sereno, 1993; Liu et al., 1998). This formulation results in a straightforward linear expression for the optimal estimate based on the EEG and/or MEG data at each time point (equation 4, below). Our previous simulation studies suggest that some care must be taken to avoid overconstraining the solution, as minor mismatches between the electrical and hemodynamic signals can then severely distort the resulting estimates (Liu et al., 1998; Liu, 2000). These studies further suggest that by using the fMRI data as a partial constraint (i.e., allowing some electrical activity in locations with no detectable fMRI response), one can obtain accurate estimates of electrical activity from MEG and EEG, even in the presence of some spatial mismatch between the generators of EEG/MEG data and the fMRI signals.

Uncertainties and Potential Errors in the Activity Estimates

It is important to note that estimates of brain structure or function based on any noninvasive imaging technology, whether based on MRI, CT, PET, SPECT, or EEG/MEG, are necessarily inexact. This imprecision is caused by several factors, including (1) noise in the measured signals, resulting in errors in the estimates; (2) errors in our model of the coupling between the parameters of interest (e.g., electrical activity, tissue perfusion, blood flow, or oxygenation) and the measured signals; and (3) fundamental ill-posedness or ambiguity of the inverse problem, resulting in limited resolution in the estimates. Thus, in order to properly interpret noninvasive imaging results, it is essential to have quantitative measures of the uncertainties and potential errors due to these different factors.

Due to the linear nature of the inverse estimation approach considered here, we can obtain a straightforward expression for the uncertainty in our activity estimates due to noise in the EEG/MEG recordings (equation 5). By normalizing the activity estimates at each location in the brain by the noise sensitivity (the standard error of the estimate), we obtain statistical parametric maps of activity at every timepoint, with millisecond accuracy (equations 6 and 7). These dynamic statistical parametric maps can be displayed as movies of brain activity over time, with each frame in these movies indicating if a statistically significant signal is present at a each cortical location at that latency.

One common and straightforward way to quantitate the spatial resolution, or degree of "blurring," at different locations in the maps is by calculating the spatial pointspread function. This function is simply the image one would obtain if all the activity were concentrated at a given point, assuming no noise in the EEG/MEG signals. Due to the time-invariant and spatially linear nature of our estimation method, one can derive a simple expression for the pointspread at every location in the brain (equation 8, below). Moreover, the spatial blurring of any arbitrary spatiotemporal activation pattern can be predicted as the activation-weighted linear superposition (sum) of the pointspread for each location and time point.

Figure 1 shows the pointspread function for three different locations (indicated by green circles), when the electrical activity is constrained to lie on the cortical surface. The left side shows the pointspread functions for the commonly used minimum norm solution (Hämäläinen and Ilmoniemi, 1984), calculated assuming 122 channels of MEG recordings. This illustrates a common problem with distributed dipole solutions, namely their tendency to misattribute focal, deep activations to extended, superficial patterns (Hämäläinen and Ilmoniemi, 1984; Dale and Sereno, 1993). The first point (top), located deep in the insula, has a particularly large point spread, covering more than half the lateral extent of the brain. The second point (middle), also located in a sulcus, has a somewhat smaller pointspread, but there is a pronounced bias toward superficial locations, as evidenced by the shift in center-of-mass away from the actual location. The third point (bottom), located more superficially near the crown of a gyrus, has a much smaller pointspread. Note that the pointspread for the noise-normalized anatomically constrained estimates, shown on the right in Figure 1, is of much more uniform extent for the different locations. (See Liu, 2000 for a more extensive analysis of the pointspread properties of different estimation approaches.)

This point is further illustrated in Figure 2, which shows pseudo-color maps and histograms of pointspread extent for all locations on the cortical surface. Again, the pointspread extent (in terms of half-width-half-max) for the minimum norm estimator varies greatly across different locations on the cortical surface, reaching as much as 100 mm or more in certain locations (shown in bright yellow). The noise-normalized estimator, on the other hand, results in a much more spatially uniform pointspread extent, with values averaging around 20 mm. A further reduction in pointspread extent can be achieved

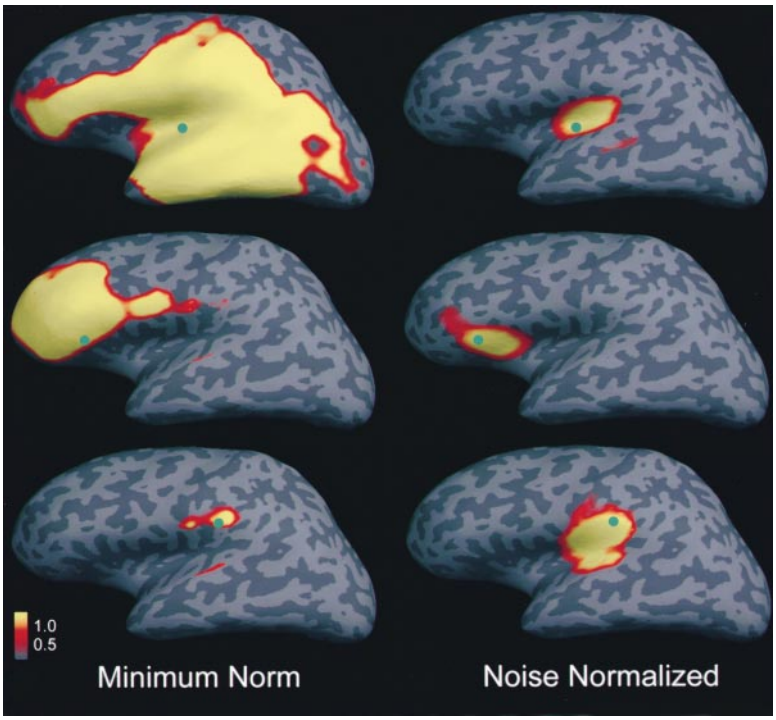

Figure 1. Spatial Resolution of the Anatomically Constrained Estimates for Three Modeled Dipole Locations

The spatial resolution of the described noise-normalized method is contrasted with that of the standard minimum norm approach (right and left columns, respectively). Shown are pointspread maps for three different dipole locations (indicated by green dots). Note that the pointspread maps for the deep dipole locations (first and second rows) are much more extensive with the minimum norm than with the noise-normalized estimator. Conversely, the pointspread map for the superficial dipole location (third row) is somewhat more focal with the minimum norm estimator. In all cases, estimates were calculated constraining activation to the cortical surface.

by increasing the number of MEG sensors and by including EEG measurements in the estimation (Liu, 2000).

Note that due to the linear nature of the estimation approach, such pointspread maps provide a direct quantitation of the local degree of spatial blurring expected in the spatiotemporal maps calculated with this method for arbitrary activation patterns. Importantly, these pointspread functions can be used to assess the spatial accuracy of the anatomically constrained estimates obtained in cognitive experiments, as described below.

Spatiotemporal Mapping of Brain Activity in a Cognitive Task

In the following, we describe the results of applying the methods described above to spatiotemporally map the activity evoked during a task involving semantic processing of visually presented words. Subjects were required to decide whether each word referred to an object or animal that is usually more than one foot in size (in any dimension). The words were either novel (i.e., presented only once in the task) or were repeated multiple times.

Anatomically Constrained Estimates Based on MEG (aMEG) in a Single Subject

Applying the anatomically constrained noise-normalized estimation procedure to the event-related MEG averages, we computed spatiotemporal activity estimates for the novel and repeated word conditions. Snapshots of these aMEG "movies" are shown in Figure 3 for four

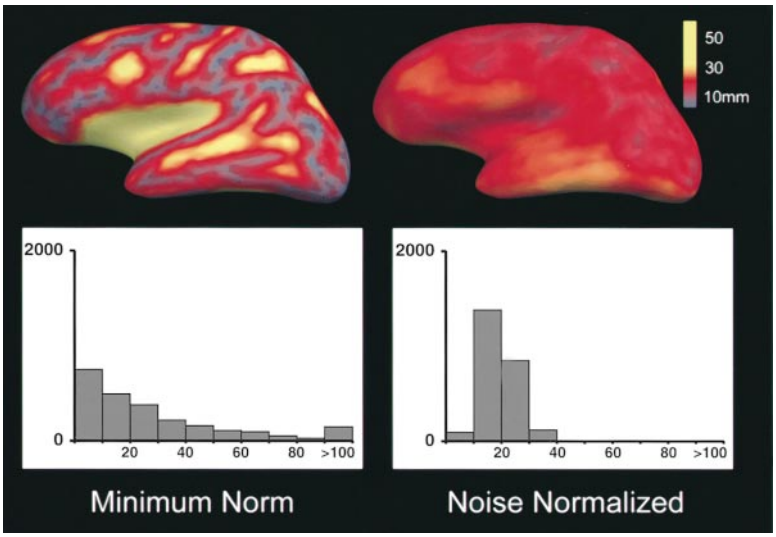

Figure 2. Spatial Resolution of the Anatomically Constrained Estimates for all Cortical Locations

Maps and histograms of pointspread extent, in terms of half-width-half-maximum in millimeters on the cortical surface, are shown for the minimum norm and noise-normalized estimators (left and right side, respectively). Note that the noise-normalized estimator results in much more spatially uniform and overall lower pointspread extent than the minimum norm estimator, particularly for deep (sulcal) locations.

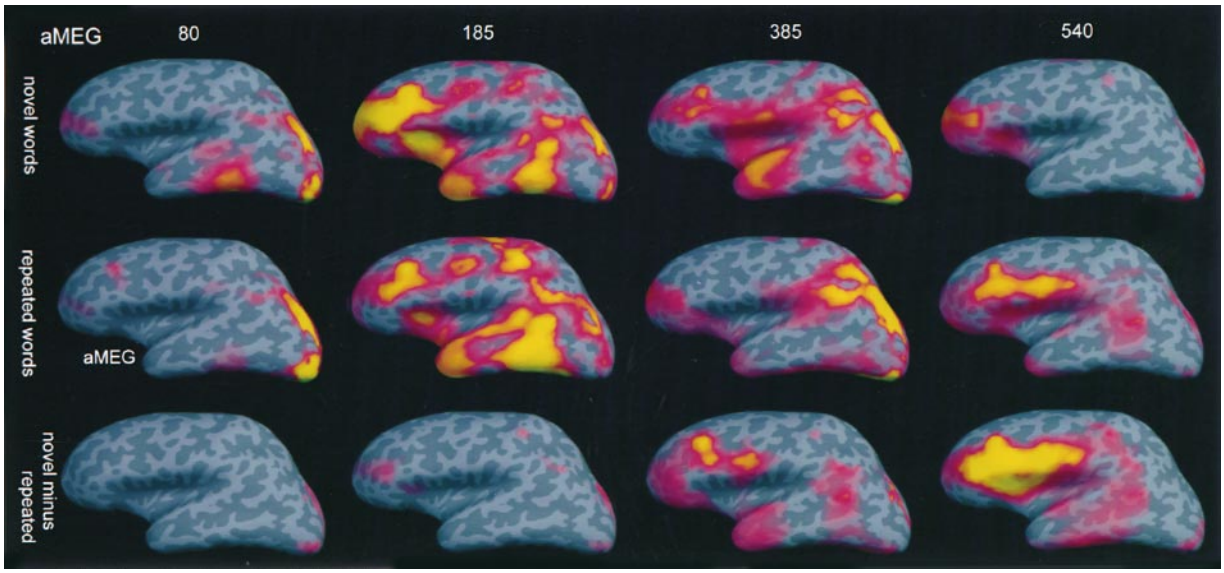

Figure 3. Snapshots of Estimated Cortical Activity at Four Representative Latencies in a Single Subject

Statistical parametric maps calculated from MEG during a verbal size judgement task are shown of the noise-normalized anatomically constrained dipole amplitudes. Activation was seen to spread rapidly from visual cortex around 80 ms to occipitotemporal, anterior temporal, and prefrontal areas. At longer latencies, activity diverged between novel and repeated words, especially in the prefrontal cortex. Activations are displayed on an "inflated" view of the left hemisphere. Sulcal and gyral cortex are shown in dark and light gray, respectively. The significance threshold for the dynamic statistical parametric maps is $p < 0.001$.

different latencies. The initial activation patterns evoked by novel words were quite similar to those evoked by repeated words. In both cases, the earliest activation was found near the foveal representation of retinotopic visual cortices beginning about 80 ms after stimulus onset. By 185 ms, activation had spread anteriorly to ventral occipitotemporal areas, the intraparietal sulcus, and the ventrolateral prefrontal cortex. Thus, within about 100–150 ms of the initial cortical activation, a widespread network encompassing many areas of the brain had been activated by both novel and repeated words. Approximately 250 ms poststimulus, the response to novel and repeated words began to clearly diverge. Activity elicited by repeated words rapidly decreased in several areas, most prominently in prefrontal cortex. The greater prefrontal activation to novel words peaked at about 385 ms, then declined and was replaced with a greater response to repeated words at a latency of about 540 ms.

fMRI to Words in a Single Subject

The left panel of Figure 4 shows the areas with significantly different fMRI signal when comparing the active task conditions described above to fixation on a stationary crosshair. Many areas were found to be involved in this task, including cortex in the occipital pole, ventral occipitotemporal junction, intraparietal sulcus, planum temporale, posterior subcentral sulcus, precentral gyrus, and ventral prefrontal areas. These results are consistent with previous PET and fMRI studies of semantic processing of visually presented words (Buckner and Koutstaal, 1998; Fiez and Petersen, 1998). A subset of

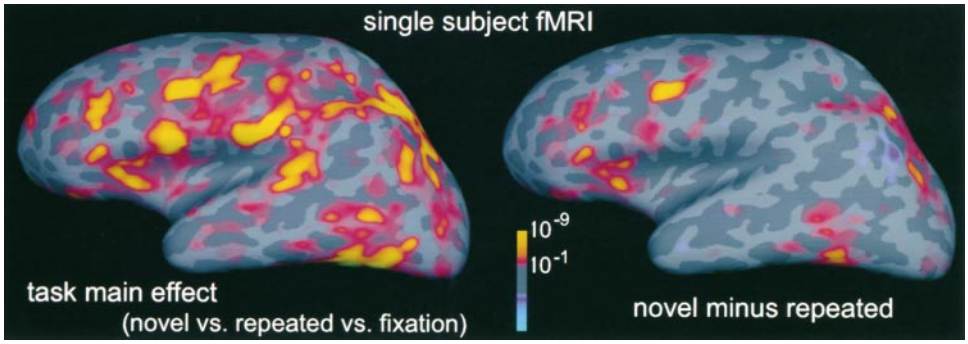

Figure 4. Location of fMRI Responses during Word Reading in a Single Subject

Areas in all lobes were found to produce significantly different fMRI responses between conditions (left panel). Many of these areas were also found to respond differently to novel versus repeated words (right panel). The fMRI activation maps are painted onto an "inflated" view of the left hemisphere of the same subject. Sulcal and gyral cortex are shown in dark and light gray, respectively.

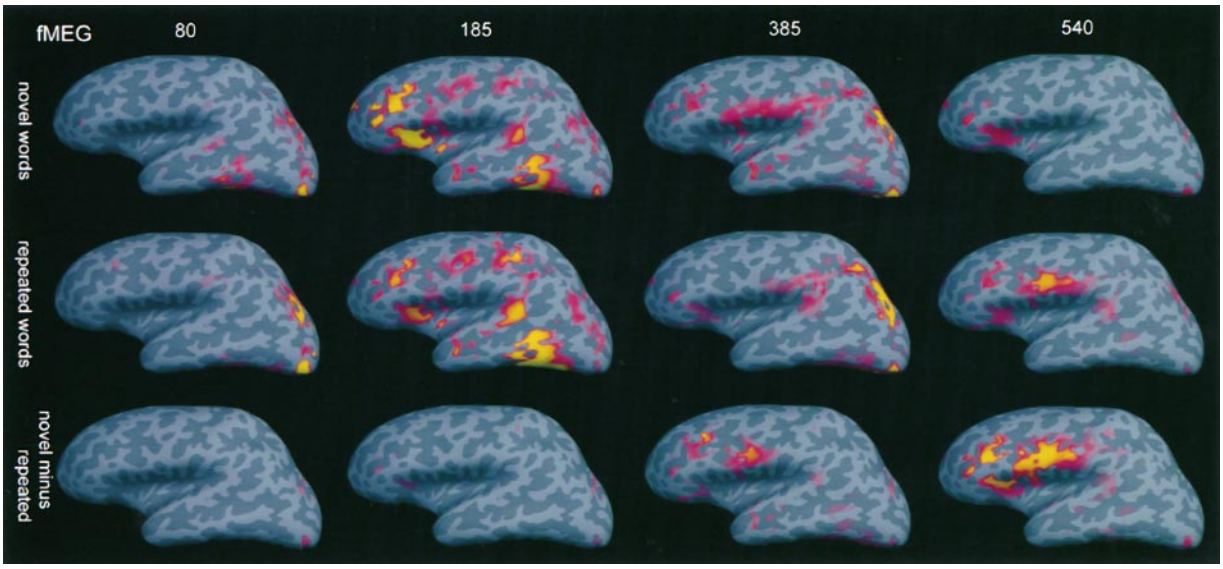

Figure 5. Snapshots of fMRI-Biased Cortical Activity Estimated from MEG at Four Different Latencies in a Single Subject

The sequence of activity in the fMRI-biased estimates were generally similar to those constrained by anatomy alone (Figure 3), with activity spreading rapidly from visual cortex to occipitotemporal, anterior temporal, and prefrontal areas. However, the fMRI-biased estimates were considerably more focal. All activations are significant for both fMRI ($p < 0.1$) and MEG ($p < 0.001$).

these areas (Figure 4, right panel) showed a decrease in activation to repeated as compared to novel words, including the occipitotemporal, intraparietal, and ventral prefrontal cortices. Note that this repetition effect was not global in that several of the areas that were found to be activated by the task, including occipital areas, the planum temporale, posterior subcentral sulcus, and precentral gyrus were not found to be affected by repetition. Again, these results are consistent with previous studies of the effects of verbal stimulus repetition on fMRI or PET activation (Raichle et al., 1994; Buckner and Koutstaal, 1998; Gabrieli et al., 1998).

Note that the anatomically constrained activity estimates (in Figure 3) and fMRI maps were calculated completely independently of each other. Thus, the generally similar distribution of activated areas derived from MEG (Figure 3) as compared to those derived from fMRI (Figure 4) in the same subject and task provides some confirmation of the spatiotemporal estimation approach. However, the spatial accuracy of the anatomically constrained estimates (limited by the estimator pointspread, as shown in Figures 1 and 2) may not be sufficient to answer many questions in cognitive neuroscience.

fMRI-Biased Estimates Based on MEG (fMEG) in a Single Subject

In order to improve the spatial resolution of the spatiotemporal activity estimates, we used fMRI to bias the solution toward hemodynamically activated areas, as described above. Snapshots of the fMEG "movies" are

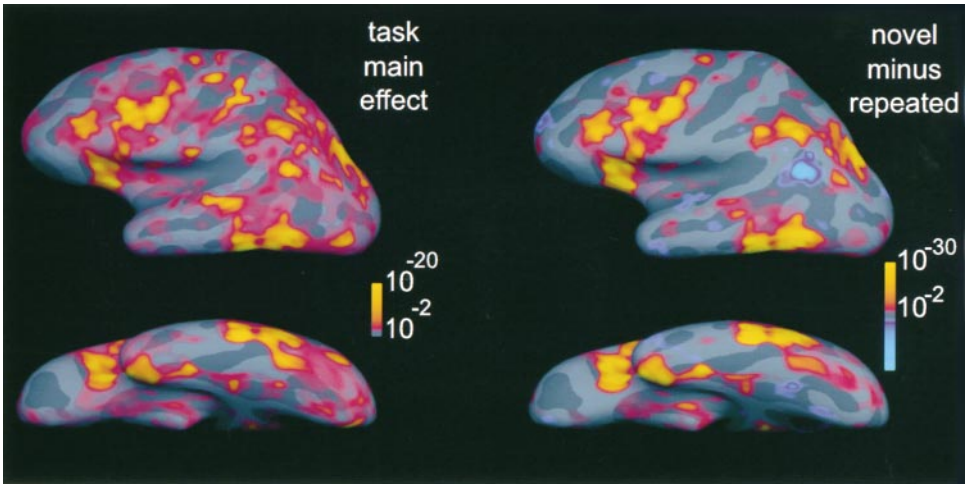

Figure 6. Grand Average Maps of fMRI Responses to Novel and Repeated Words

fMRI responses were averaged across four subjects using a cortical surface-based morphing procedure and displayed on an averaged curvature pattern. A widely distributed cortical network was found to be reponsive to the task conditions, with repetition effects observed in the activity in prefrontal, medioventral temporal, intraparietal, and supplementary motor cortices.

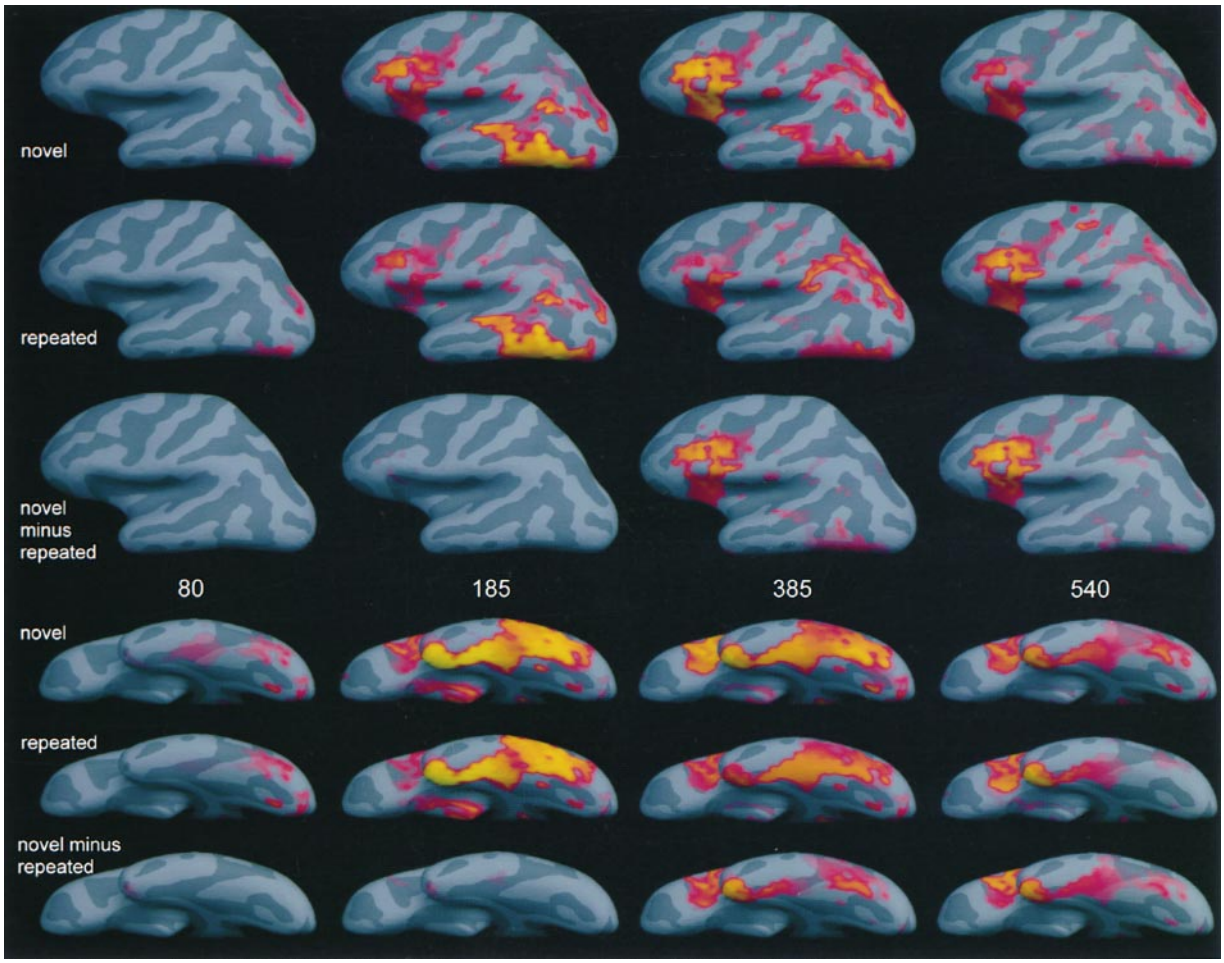

Figure 7. Snapshots of Grand Average fMRI-Biased Cortical Estimated from MEG at Four Different Latencies

fMRI-biased spatiotemporal activity estimates were averaged across four subjects. Activity was found to spread very rapidly from the occipital pole at 80 ms, to the medioventral temporal lobe at 100 ms, and then to lateral inferotemporal, intraparietal, prefrontal, anterior cingular cortices at 185 ms. These areas remained active for about 400 ms. By 250 ms after stimulus onset, activity in the medial temporal lobe was greater to novel than to repeated words. At 385 ms, this repetition effect had spread to prefrontal and anterior cingular cortices. All activations are significant for both fMRI ($p < 0.01$) and MEG ($p < 0.001$).

shown in Figure 5 for the same four latencies as shown in Figure 3. Overall, the fMRI bias resulted in a substantial focusing of the activation relative to the anatomically constrained MEG estimates. The general sequence of activation appeared quite similar in the fMRI-biased and anatomically constrained MEG estimates, with an initial activation in visual cortex, spreading rapidly to temporal and frontal areas. Furthermore, the repetition effects again involve primarily occipitotemporal and prefrontal cortices, starting around 250 ms poststimulus onset. Note that since the same fMRI bias was used in all fMRI-biased estimates (for novel, repeated, and novel-repeated), any differences between the task conditions are due exclusively to the differences between the MEG signals in these conditions.

Across-Subject Averages of fMRI-Biased Spatiotemporal Estimates

Cortical activation estimates were averaged across four subjects using a surface-based morphing procedure in order to achieve improved alignment of corresponding anatomical features across individuals (Fischl et al., 1999b). The SPMs for the grand averaged fMRI data, shown in Figure 6, again show that the task involves a large number of areas. As for the individual subject displayed in Figure 5, these fMRI data were used to bias the MEG inverse solution in the same four subjects, and the resulting fMRI-biased estimates were averaged across subject using surface alignment.

Selected frames from the resulting "movies," shown in Figure 7, confirmed the basic results already described for a single subject but also revealed additional details. The patterns of activation were nearly identical for novel and repeated words for the initial 200 ms. The earliest activation, by about 80 ms, was noted near the occipital pole, and by 100 ms, activity had spread anteriorly along the medioventral temporal lobe to the rhinal cortex. At 185 ms, the estimated activity in the occipital pole had already declined, while activity in the entire extent of the medioventral temporal lobe had become much stronger, and new foci of activation appeared in occipitotemporal, prefrontal, and anterior cingulate cortices. Occipitotemporal activation declined by 385 ms, whereas prefrontal activation continued to increase,

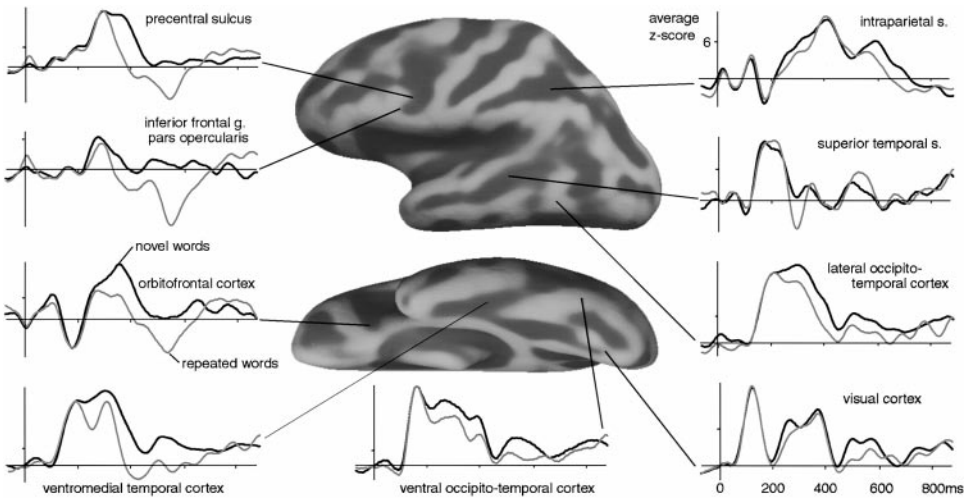

Figure 8. Estimated Time Courses of Cortical Areas Responsive to Processing of Novel and Repeated Words

The fMRI-biased time courses estimated from MEG, normalized for noise sensitivity, were averaged across four subjects (as in Figure 7). Black lines show the response to novel words, and gray lines the response to repeated words. Waveforms are derived from single cortical locations (each one representing about 0.5 cm^2). A z-score of 6 corresponds to a significance level of $p < 10^{-8}$.

at least to novel words. Note again that since the same fMRI bias was used in all the fMRI-biased estimates, any differences between the task conditions or at different latencies are due exclusively to the MEG signals. By partially constraining the inverse solution, the fMRI bias helps to manifest the localizing information that is inherent in the distribution of MEG signals across the sensors.

The location of the earliest detectable activity at 80 ms corresponds to early retinotopic visual areas previously studied with fMRI (Sereno et al., 1995), and the latency of this estimated response corresponds to the onset latency of the EEG and MEG responses evoked by simple visual stimuli (Regan, 1989; Portin et al., 1998; Martinez et al., 1999). The rapid spread of fMEG activation to rhinal cortex and then prefrontal cortices are consistent with direct intracranial EEG (iEEG) responses to visual words and faces (Halgren et al., 1994a, 1994b).

Previous studies have suggested that the occipitotemporal cortex is concerned with midlevel form vision (Ungerleider and Mishkin, 1982), rhinal cortex with complex stimulus integration with memory and emotion (Amaral et al., 1992; Halgren, 1994; Halgren and Marinkovic, 1995; Murray and Bussey, 1999), and the ventrolateral prefrontal cortex with working memory (Gabrieli et al., 1998). Thus, the current data suggest that high-level association areas are coactivated with perceptual areas in processing an event from a relatively early stage. Other areas that are coactivated include ones thought to be involved in lexical access (supramarginal and superior temporal cortex) (Benson, 1979), attentional control (intraparietal cortex) (Mesulam, 1990; Corbetta, 1998), and motor response organization (medial frontal cortex) (Picard and Strick, 1996). These results are difficult to reconcile with a discrete sequential activation of successive cognitive processing modules. In particular, these data argue against theories of prefrontal function that posit its involvement only following the encoding of the event by posterior association and perceptual cortices.

The more rapid decline from peak activity in response to repeated words resulted in clear repetition effects visible by 250 ms in the left medioventral temporal cortex (Figure 7). These differences were considerably stronger by 385 ms, when they also included prefrontal and cingulate areas. A second peak of repetition effects occurred at 540 ms, when activity was greater to repeated words in most areas. Note that many of the occipital, parietal, and perirolandic areas showing strong and sustained activation to words did not show clear repetition effects. Repetition effects appeared much stronger in the left hemisphere than in the right, although their general location was similar. Activation remained close to baseline levels from about 670 ms poststimulus onset.

The snapshots of the fMRI-biased spatiotemporal estimates show estimated activity over the entire lateral aspect of the cortical surface of the left hemisphere at selected moments in time (Figure 7). An alternative method for examining the data is to plot the estimated dipole strength at selected locations at all latencies (Figure 8). These time courses support the same general points made by the movie snapshots: (1) activation began in retinotopic visual cortex and spread very rapidly anteriorly; (2) activation appeared to be identical for novel and repeated stimuli during the initial 200–260 ms, depending on the site; (3) the repetition effects do not involve all areas equally; and (4) the repetition effect evolves only gradually in a widespread network.

In summary, repetition effects are widespread and occur only after the initial activation of the entire network. The locations of the cortical areas found to be affected by stimulus repetition using fMRI-biased MEG estimation are consistent with the findings of previous PET and fMRI studies (Buckner and Koutstaal, 1998). Similarly, the timing of the fMEG signals that change with repetition resemble the N4/LPC components recorded in many previous EEG studies (Kutas and Van Petten, 1988; Halgren, 1990, 1994). Furthermore, both the localization and the timing of repetition-induced

changes in the fMRI-biased estimates correspond very closely to those of the generators of the N4/LPC, as identified in previous intracranial EEG studies in word repetition and semantic priming tasks (Smith et al., 1986; Halgren et al., 1994a, 1994b; Nobre et al., 1994; McCarthy et al., 1995; Nobre and McCarthy 1995; Fernandez et al., 1999; Guillem et al., 1999).

In addition to this global similarity in generating structures, there is a close correspondence between the usual waveforms found in these previous iEEG studies and the fMEG waveforms reported here. The fMRI-biased estimates of the response to novel versus repeated stimuli showed two maxima, at about 385 and 540 ms after stimulus onset, consistent with what would be expected in the same task for the N4 and LPC, respectively. Like the fMRI-biased estimate, the repetition effect associated with the N4/LPC extends from about 250 to 650 ms. The first fMEG peak was due to greater activity evoked by novel words, and the second was due to greater activity evoked by repeated words. Similarly, N4 amplitude declines and the LPC increases when a word is repeated. The similarity to intracerebral recordings provides an especially strong validation of the fMRI-biased activity estimates, as intracerebral EEG recordings can provide reasonably localized estimates of the time course of the net dipolar current flows within a volume of tissue around the electrode contacts.

Limitations and Future Improvements

Although the simulations and experimental data presented here involve only MEG recordings, it should be noted that the methods are equally applicable to EEG or combined EEG/MEG recordings. In fact, by combining both kinds of recordings, it is possible to substantially improve the accuracy of the anatomically constrained estimates in certain situations (Dale and Sereno, 1993; Liu, 2000). The main challenge in including EEG data in the analysis is to obtain a sufficiently accurate forward solution, given the greater dependence of the EEG signal on the exact head shape and the conductivities of different tissue types (Nunez, 1981; Hämäläinen and Ilmoniemi, 1984).

In the preceding analyses, dipole activity was assumed to be limited to the cortical surface (including the hippocampus as well as the neocortex). While it is possible for subcortical structures such as the lateral geniculate body to produce dipolar current source distributions (Schroeder et al., 1995), the MEG signals from these structures tend to be of shorter latency and duration and smaller amplitude relative to cortical signals (Gobbele et al., 1998). In cognitive experiments, where one is focusing on the later, large-amplitude signals lasting hundreds of milliseconds, it is thus unlikely that subcortically generated signals are much of a factor. However, for sensory experiments, particularly when EEG signals are included in the analysis, it may be important to extend the anatomical source model to also take into account possible subcortical generator structures.

In order to further improve the accuracy of the fMRI-biased estimates (fMEG), a better understanding of the coupling between the observed hemodynamic response, as measured by the blood oxygenation level dependent (BOLD) signal, and the local current dipole activity over time is needed. Using fMRI and/or optical imaging methods in humans and animals along with cortical laminar recordings, it may be possible to obtain a more precise, quantitative model of this coupling. Recordings with multicontact laminar electrodes and 2D surface grids can also provide a better understanding of the spatiotemporal patterns of synaptic current flow in the cortex at micro- and mesoscopic scales (Nicholson and Freeman, 1975; Barth and MacDonald, 1996). Since the observed MEG/EEG signals are directly related to these synaptic current flows (the dipole moment is the first nonvanishing term of the multipolar expansion of the laminar current source density distribution), this information could lead to greatly improved constraints on the spatiotemporal activity estimates. Ultimately, this would allow noninvasive measures like EEG, MEG, and fMRI to be used to test biophysical models of cortical neuronal circuitry.

Experimental Procedures

Integration of Imaging Modalities

The goal of the current approach is to determine the spatiotemporal pattern of electrical activity that is most consistent with all observables (e.g., EEG, MEG, and fMRI) as well as a priori information. Formally, this can be posed as a problem of computing the solution with the maximum a posteriori probability, given by Bayes Formula as

$$P(\mathbf{j}(\mathbf{r},t)|\mathbf{x}(t)\ \&\ f(\mathbf{r},t)) = \frac{P(\mathbf{x}(t)|\mathbf{j}(\mathbf{r},t))P(f(\mathbf{r},t)|\mathbf{j}(\mathbf{r},t))P(\mathbf{j}(\mathbf{r},t))}{P(\mathbf{x}(t)\ \&\ f(\mathbf{r},t))}, \quad (1)$$

where $\mathbf{j}(\mathbf{r},t)$ denotes the current dipole vector, $\mathbf{x}(t)$ denotes the vector of EEG/MEG recordings, and $f(\mathbf{r},t)$ denotes the fMRI signal at location $\mathbf{r}$ and time point t. The term $P(\mathbf{x}(t)|\mathbf{j}(\mathbf{r},t))$ in equation 1 represents the relationship between the spatiotemporal pattern of dipole strength and the recorded EEG and/or MEG data, commonly referred to as the forward solution. In the frequency range of typical EEG/MEG recordings (typically $<<$ 1000 Hz), the forward solution has a simple, linear form, given by

$$\mathbf{x}(t) = \int_S \mathbf{G}(\mathbf{r})\mathbf{j}(t,\mathbf{r})d\mathbf{r} + \mathbf{n}(t), \quad (2)$$

where S denotes the space of (possible) dipole source locations, the three columns of the matrix $\mathbf{G}(\mathbf{r})$ specify the predicted EEG/MEG recording vector for the three dipole components at location $\mathbf{r}$, and $\mathbf{n}(t)$ denotes additive noise. For computational purposes, the source space S is typically divided into a set of discrete elements, with dipole components representing the local current dipole within a small region. Equation 2 can then be written as

$$\mathbf{x}(t) = \mathbf{A}\mathbf{s}(t) + \mathbf{n}(t), \quad (3)$$

where $\mathbf{s}(t)$ denotes a vector of dipole component strengths, and the $\mathbf{A}$ denotes the resulting linear forward matrix operator (Dale and Sereno, 1993). The term $P(f(\mathbf{r},t)|\mathbf{j}(\mathbf{r},t))$ in equation 1 similarly encodes the coupling between the spatiotemporal pattern of electrical activity (in terms of dipole strength) and the fMRI signal. Finally, the term $P(\mathbf{j}(\mathbf{r},t))$ encodes a priori information about the solution, i.e., the likelihood of different spatiotemporal patterns of dipole strength. This provides a mechanism for incorporating knowledge of spatial correlations in electrical activity within different brain structures.

As discussed above, little quantitative data exist regarding the coupling between electrical activity and hemodynamic response. However, there is strong evidence for a general correlation between the spatial pattern of electrical activity and hemodynamic measures. This suggests that one can use the measured fMRI response to spatially bias the estimate of electrical activity over time. Specifically, one may assume that areas that show a strong fMRI response are more likely to be electrically active. Assuming that the prior information about dipole strength patterns can be expressed in terms of a multivariate Gaussian distribution, it can be shown that

the maximum a posteriori probability (MAP) estimate is equivalent to the linear Wiener estimate given by

$$\hat{\mathbf{s}}(t) = \mathbf{W}\mathbf{x}(t), \text{ where } \mathbf{W} = \mathbf{R}\mathbf{A}^T(\mathbf{A}\mathbf{R}\mathbf{A}^T + \mathrm{C})^{-1}, \quad (4)$$

where $\mathbf{C} = <\mathbf{n}(t)\mathbf{n}(t)T>$ is the spatial (sensor) covariance matrix of the noise, and $\mathbf{R} = <\mathbf{s}(t)\mathbf{s}(t)^T>$ is the spatial covariance matrix of the dipole strength vector (Dale and Sereno, 1993; van Oosterom, 1999). If one further assumes that the dipole strength variance (or power) over time can be expressed as a function of the local fMRI response, this information can be encoded in the diagonal elements of **R** (Dale and Sereno, 1993). Information about the spatial covariance of dipole strength (i.e., spatial smoothness) can similarly be encoded in the off-diagonal elements of **R**.

One straightforward way to implement the fMRI constraint is to simply threshold the fMRI statistical parametric map and set the a priori variance estimate to a nonzero value only at locations exceeding a certain threshold (George et al., 1995). However, simulation studies suggest that this approach is exceedingly sensitive to minor model misspecifications, in particular to the presence of generators of EEG or MEG signals that are not detected by fMRI (Liu et al., 1998; Liu, 2000). These studies suggest that the distorting effect of such potential misspecifications is greatly reduced by imposing a partial fMRI constraint or bias. This is accomplished by setting the minimum a priori variance estimate to some finite, nonzero value (typically 10% of the maximum value).

Dynamic Statistical Parametric Mapping

Typically, MEG and EEG are modeled as resulting from the activity of discrete equivalent current dipoles with time-varying moment and orientation. In contrast, tomographic methods like fMRI provide signal estimates at every location within a volume. Because the noise variance may vary greatly between voxels, fMRI activation estimates are usually presented as noise-normalized statistical parametric maps (SPMs), rather than as maps of raw signal strength. The current method provides activity time course estimates for every cortical location. By normalizing these estimates by predicted estimator noise, one can similarly obtain noise normalized SPMs for each time point.

Due to the linear nature of the Wiener estimate defined in equation 4, it is straightforward to compute the variance of each dipole strength estimate due to the additive noise. Specifically, we have

$$Var(\hat{s}_i) = <(\mathbf{w}_i\mathbf{n}(t))^2> = \mathbf{w}_i\,\mathbf{C}\mathbf{w}_i^T, \quad (5)$$

where $\hat{s}_i$ denotes the i^{th} element of the dipole strength vector $\hat{\mathbf{s}}$, and $\mathbf{w}_i$ denotes the i^{th} row of the inverse operator **W** (Liu, 2000). Note that in general three dipole components are required to represent an arbitrary dipole orientation and strength at each location in the brain. For locations whose dipole orientation are known a priori based on anatomical information, only the dipole strength needs to be determined for each location (Dale and Sereno, 1993). In this case, a noise-normalized activity estimate $z_i(t)$ can be computed for each time point t and location i as follows

$$z_i(t) = \frac{\mathbf{w}_i \cdot \mathbf{x}(t)}{\sqrt{\mathbf{w}_i\,\mathbf{C}\mathbf{w}_i^T}}, \quad (6)$$

where **C** is, again, the estimated noise covariance matrix (Dale and Sereno, 1993; Liu et al., 1998). By dividing the estimated total dipole strength estimate for each location (the numerator in equation 6) by the predicted standard error of the estimate due to additive noise (the denominator in equation 6), we obtain a normalized dipole strength $z_i(t)$ that is t distributed under the null hypothesis of no dipole activity (i.e., $\mathbf{s}(t) = 0$). Since the number of time samples used to calculate the noise covariance matrix **C** is quite large (typically more than 100), the t distribution approaches a unit normal distribution (i.e., a z-score).

If, on the other hand, no a priori assumptions are made about the local dipole orientation, three components are required for each location. A noise-normalized estimate of the local current dipole power (sum of squared dipole component strengths) at location i is given by

$$q_i(t) = \frac{\sum_{j \in G_i} (\mathbf{w}_j \cdot \mathbf{x}(t))^2}{\sum_{j \in G_i} \mathbf{w}_j\,\mathbf{C}\mathbf{w}_j^T}, \quad (7)$$

where G_i is the set of (three) dipole component indices for the i^{th} location. Note that under the null hypothesis, $q_i(t)$ is F distributed, with three degrees of freedom for the numerator. The degrees of freedom for the denominator is typically large, again depending on the number of time samples used to calculate the noise covariance matrix **C**.

Analysis of Spatial Resolution

An important property of linear estimation approaches is the existence of an explicit expression for the spatial resolution of the dipole strength estimates at every location in the source space. Due to the linear nature of both the forward and inverse solutions, represented by linear operators **A** and **W**, respectively, the estimated dipole strength vector $\hat{\mathbf{s}}(t)$ can be expressed as a linear operation on the actual dipole strength vector $\mathbf{s}(t)$. More precisely,

$$<\hat{\mathbf{s}}(t)> = <\mathbf{W}\mathbf{x}(t)> = <\mathbf{W}\mathbf{A}\mathbf{s}(t) + \mathbf{W}\mathbf{n}(t)> = \mathbf{W}\mathbf{A}\mathbf{s}(t). \quad (8)$$

The matrix **WA** is commonly referred to as a resolution matrix, where the columns specify the pointspread for each dipole location, i.e., the spatial pattern of estimated dipole strength for a unit of actual dipole strength at a particular location (Menke, 1989; Dale and Sereno, 1993; Press et al., 1994; Grave de Peralta Menendez et al., 1997). The half-width-half-max measure was determined by computing the average distance to the dipoles at which the estimated dipole strength was greater than half its value at the point where the model dipole was actually placed.

Cognitive Task

A total of 370 concrete nouns, 3–11 letters long, representing objects and animals were used as stimuli. Each word was presented for 240 ms with a 1600 ms stimulus onset asynchrony on a back-projection screen using an LCD video projector. The subject pressed a key with his/her right hand if the object or animal that the word represented was usually more than a foot in its longest dimension. The task was performed by the subjects with each of the repeated words six times before data collection began. Stimulus blocks were presented in a fixed order of novel-fixation-repeated-fixation. Three hundred sixty of the words were shown only once in one of the novel blocks and ten words were presented repeatedly in the repeated blocks. In the repeated blocks, each of the ten repeated words was presented once but in a different order within each block. Active blocks were separated by 16 s of visual fixation. Thus, a given repeating word occurred once and only once in each repeated block, and an average of 64 s and 19 intervening stimuli passed between successive presentations of the same word. In each of nine runs, four blocks of repeated words and four of novel were presented. Animals and objects were presented in separate runs. Across runs presenting animals (objects), the same ten animals (objects) were used as repeating stimuli. Exactly the same tasks were used for fMRI and MEG studies, with overlapping stimulus lists. Approximately six months passed between fMRI and MEG testing sessions.

Physiological Data Acquisition and Analysis

The same four normal, strongly right-handed, young adults (one male) were studied with MRI, fMRI, and MEG after appropriate informed consent. The structural MRI was acquired on a 1.5 T Siemens Vision scanner using an MPRAGE sequence (TR = 9.7 ms, TI = 20 ms, TE = 4 ms, flip angle = 10°, FOV = 256 mm, slice thickness = 1 mm), and the cortical surface was reconstructed as described below.

fMRI data were collected using a GE 1.5 T MRI scanner retrofitted for echoplanar imaging (Advanced NMR Systems, Wilmington, MA). Data were acquired from 16 approximately axial slices covering the entire brain (7 mm slice thickness; 3.1 × 3.1 mm in-plane resolution) using a standard GE quadrature head coil. An automated shimming procedure was used to improve B_0 field homogeneity (Reese et al., 1995). T1-weighted inversion recovery echoplanar images were acquired for anatomical alignment of functional images (TR = 20 s,

TI = 1100 ms, 1.5625 mm in-plane resolution). Finally, T2*-weighted functional images were acquired using an asymmetric spin echo sequence sensitive to BOLD contrast (tau = −25 ms, TE = 50 ms, TR = 2000 ms, 3.125 mm in-plane resolution). The fMRI data were analyzed using a generalized linear model, where the fMRI signal was modeled as a piecewise constant function of experimental condition (novel, repeated, and fixation) convolved with an assumed impulse response function (Boynton et al., 1996; Friston et al., 1998). This model was used to obtain statistical parametric maps for the main effect of experimental condition (using an F test) as well as for the comparison of the response to different conditions, including novel words versus fixation and novel versus repeated words (using a t test). Activation from the four subjects was averaged by aligning each subject's sulcal pattern to the average of a group of 35 normal subjects (see above).

MEG signals were recorded from 0.3 to 20 Hz using a 122 channel planar dc-SQUID gradiometer system covering the entire scalp (Hämäläinen et al., 1993). Trials with eyeblinks or other artifacts were rejected from analysis.

Cortical Surface Reconstruction

Geometrical representations for the cortical surfaces of each subject were obtained using procedures described in detail in Dale et al. (1999) and Fischl et al. (1999a). First, high-resolution 3D T1-weighted structural images were acquired for each subject. Then, a segmentation of cortical white matter was performed, and the estimated border between gray and white matter was tessellated, providing a triangular representation of the surface. This representation of the folded cortical surface was used to derive the locations and orientations of the dipoles used in the analysis of the MEG data (see below). Finally, the folded surface tessellation was "inflated" in order to unfold cortical sulci, thereby providing a convenient format for visualizing cortical activation patterns (Dale et al., 1999; Fischl et al., 1999a). For purposes of intersubject averaging, the reconstructed surface for each subject was then morphed into an average spherical representation, optimally aligning sulcal and gyral features across subjects while minimizing metric distortion (Fischl et al., 1999b). This nonrigid surface-based deformation procedure results in a substantial reduction in anatomical and functional variability across subjects relative to the more commonly used normalization approach of Talairach et al. (1967), thereby improving the anatomical precision of the intersubject averages.

Anatomically Constrained MEG (aMEG) and fMRI-Biased MEG (fMEG) Solutions

For aMEG and fMEG analysis, the cortical surface was first subsampled to about 2500 dipole locations per hemisphere. The forward solution for each of the three dipole components at each of these locations was calculated using a boundary element model (Oostendorp and Van Oosterom, 1992). The conductivity boundaries for this model were determined from the segmented MRI described above. The activation at each location on the cortical surface was estimated every 5 ms using the anatomically and functionally constrained linear estimation approach described above (see also Dale and Sereno, 1993; Liu et al., 1998; Liu, 2000). For aMEG analysis, the fMRI weighting was set to 0%, i.e., no fMRI constraint was used. For fMEG analysis, the fMRI weighting was set to 90%, a value suggested by our earlier simulation studies (Liu et al., 1998).

The aMEG and fMEG maps (Figures 3, 5, and 7) were calculated without constraining the dipole orientation, with the sensitivity-normalized estimates calculated according to equation 7. The regional time course estimates shown in Figure 8 were calculated using dipole orientation estimates obtained based on the cortical surface reconstruction in each subject and sensitivity normalized for each subject as specified in equation 6. The time course and the amplitude of the resulting waveforms from adjacent locations were usually highly similar due to the pointspread of the estimator (see Figure 1). However, the polarity of the waveforms commonly inverted between nearby sites with different cortical orientations and thus should be considered arbitrary.

Acknowledgments

We thank S. A. Hillyard, W. C. West, and L. Anllo-Vento for helpful comments on the manuscript. We are also grateful for the technical collaboration of K. Kwong and J. Klopp. This research was supported by the Human Frontiers Science Program (A. M. D. and E. H.), the National Foundation for Functional Brain Imaging (B. R., A. M. D., and E. H.), the Whitaker Foundation (A. M. D.), Office of Naval Research (E. H.), and the National Institutes of Health (A. M. D.: R01-RR13609; E. H.: R01-NS18741).

Received June 20, 1999; revised March 1, 2000.

References

Ahlfors, S.P., Simpson, G.V., Dale, A.M., Belliveau, J.W., Liu, A.K., Korvenoja, A., Virtanen, J., Huotilainen, M., Tootell, R.B., Aronen, H.J., and Ilmoniemi, R.J. (1999). Spatiotemporal activity of a cortical network for processing visual motion revealed by MEG and fMRI. J. Neurophysiol. *82*, 2545–2555.

Amaral, D.G., Price, J.L., Pitkänen, A., and Carmichael, S.T. (1992). Anatomical organization of the primate amygdaloid complex. In The Amygdala: Neurobiological Aspects of Emotion, Memory, and Mental Dysfunction, J.P. Aggleton, ed. (New York: Wiley-Liss), pp. 1–66.

Arieli, A., Sterkin, A., Grinvald, A., and Aertsen, A. (1996). Dynamics of ongoing activity: explanation of the large variability in evoked cortical responses. Science *273*, 1868–1871.

Barth, D.S., and Di, S. (1991). Laminar excitability cycles in neocortex. J. Neurophysiol. *65*, 891–898.

Barth, D.S., and MacDonald, K.D. (1996). Thalamic modulation of high-frequency oscillating potentials in auditory cortex. Nature *383*, 78–81.

Baudena, P., Heit, G., Clarke, J.M., and Halgren, E. (1995). Intracerebral potentials to rare target and distractor auditory and visual stimuli: 3. Frontal cortex. Electroencephalogr. Clin. Neurophysiol. *94*, 251–264.

Belliveau, J.W., Kennedy, D.N., McKinstry, R.C., Buchbinder, B.R., Weisskoff, R.M., Cohen, M.S., Vevea, J.M., Brady, T.J., and Rosen, B.R. (1991). Functional mapping of the human visual cortex by magnetic resonance imaging. Science *254*, 716–719.

Benson, D.F. (1979). Aphasia, Alexia, and Agraphia (New York: Churchill Livingstone).

Benson, R.R., Logan, W.J., Cosgrove, G.R., Cole, A.J., Jiang, H., LeSueur, L.L., Buchbinder, B.R., Rosen, B.R., and Caviness, V.S. (1996). Functional MRI localization of language in a 9-year-old child. Can. J. Neurol. Sci. *23*, 213–219.

Boynton, G.M., Engel, S.A., Glover, G.H., and Heeger, D.J. (1996). Linear systems analysis of functional magnetic resonance imaging in human V1. J. Neurosci. *16*, 4207–4221.

Buckner, R.L., and Koutstaal, W. (1998). Functional neuroimaging studies of encoding, priming, and explicit memory retrieval. Proc. Nat. Acad. Sci. USA *95*, 891–898.

Chauvel, P., Buser, P., Badier, J.M., Liégeois-Chauvel, C., Marquis, P., and Bancaud, J. (1987). The "epileptogenic zone" in humans: representation of intercritical events by spatio-temporal maps. Rev. Neurol. (Paris) *143*, 443–450.

Churchland, P.S., and Sejnowski, T.J. (1988). Perspectives on cognitive neuroscience. Science *242*, 741–745.

Corbetta, M. (1998). Frontoparietal cortical networks for directing attention and the eye to visual locations: identical, independent, or overlapping neural systems? Proc. Natl. Acad. Sci. USA *95*, 831–838.

Dale, A.M., and Sereno, M.I. (1993). Improved localization of cortical activity by combining EEG and MEG with MRI cortical surface reconstruction: a linear approach. J. Cog. Neurosci. *5*, 162–176.

Dale, A.M., Fischl, B., and Sereno, M.I. (1999). Cortical surface-based analysis I: segmentation and surface reconstruction. Neuroimage *9*, 179–194.

Fernandez, G., Effern, A., Grunwald, T., Pezer, N., Lehnertz, K., Dumpelmann, M., Van Roost, D., and Elger, C.E. (1999). Real-time tracking of memory formation in the human rhinal cortex and hippocampus. Science *285*, 1582–1585.

Fiez, J.A., and Petersen, S.E. (1998). Neuroimaging studies of word reading. Proc. Nat. Acad. Sci. USA *95*, 914–921.

Fischl, B., Sereno, M.I., and Dale, A.M. (1999a). Cortical surface-based analysis II: inflation, flattening, a surface-based coordinate system. Neuroimage *9*, 195–207.

Fischl, B., Sereno, M.I., Tootell, R.B., and Dale, A.M. (1999b). High-resolution intersubject averaging and a coordinate system for the cortical surface. Hum. Brain Mapp. *8*, 272–284.

Fox, P.T., and Raichle, M.E. (1986). Focal physiological uncoupling of cerebral blood flow and oxidative metabolism during somatosensory stimulation in human subjects. Proc. Nat. Acad. Sci. USA *83*, 1140–1144.

Fox, P.T., Raichle, M.E., Mintun, M.A., and Dence, C. (1988). Nonoxidative glucose consumption during focal physiologic neural activity. Science *241*, 462–464.

Friston, K.J., Fletcher, P., Josephs, O., Holmes, A., Rugg, M.D., and Turner, R. (1998). Event-related fMRI: characterizing differential responses. Neuroimage *7*, 30–40.

Gabrieli, J., Poldrack, R., and Desmond, J. (1998). The role of left prefrontal cortex in language and memory. Proc. Natl. Acad. Sci. USA *95*, 906–913.

George, J., Mosher, J., Schmidt, D., Aine, C., Wood, C., Lewine, J., Sanders, J., and Belliveau, J. (1995). Functional Neuroimaging by Combined MRI, MEG and fMRI. Hum. Brain Mapp. *S1*, 89.

Gobbele, R., Buchner, H., and Curio, G. (1998). High-frequency (600 Hz) SEP activities originating in the subcortical and cortical human somatosensory system. Electroencephalogr. Clin. Neurophysiol. *108*, 182–189.

Grave de Peralta Menendez, R., Hauk, O., Andino, S.G., Vogt, H., and Michel, C. (1997). Linear inverse solutions with optimal resolution kernels applied to electromagnetic tomography. Hum. Brain Mapp. *5*, 454–467.

Grinvald, A., Lieke, E., Frostig, R.D., Gilbert, C.D., and Wiesel, T.N. (1986). Functional architecture of cortex revealed by optical imaging of intrinsic signals. Nature *324*, 361–364.

Guillem, F., Rougier, A., and Claverie, B. (1999). Short- and long-delay intracranial ERP repetition effects dissociate memory systems in the human brain. J. Cog. Neurosci. *11*, 437–458.

Halgren, E. (1990). Insights from evoked potentials into the neuropsychological mechanisms of reading. In Neurobiology of Cognition, A. Scheibel and A. Weschsler, eds. (New York: Guilford), pp. 103–150.

Halgren, E. (1994). Physiological integration of the declarative memory system. In The Memory System of the Brain, J. Delacour, ed. (New York: World Scientific), pp. 69–155.

Halgren, E., and Marinkovic, K. (1995). Neurophysiological networks integrating human emotions. In The Cognitive Neurosciences, M. Gazzaniga, ed. (Cambridge, MA: MIT Press), pp. 1137–1151.

Halgren, E., Baudena, P., Heit, G., Clarke, J.M., and Marinkovic, K. (1994a). Spatio-temporal stages in face and word processing. 1. Depth-recorded potentials in the human occipital, temporal and parietal lobes. J. Physiol. (Paris) *88*, 1–50.

Halgren, E., Baudena, P., Heit, G., Clarke, J.M., Marinkovic, K., and Chauvel, P. (1994b). Spatio-temporal stages in face and word processing. 2. Depth-recorded potentials in the human frontal and Rolandic cortices. J. Physiol. (Paris) *88*, 51–80.

Halgren, E., Baudena, P., Clarke, J.M., Heit, G., Liégeois-Chauvel, C., Chauvel, P., and Musolino, A. (1995a). Intracerebral potentials to rare target and distractor auditory and visual stimuli: 1. Superior temporal plane and parietal lobe. Electroencephalogr. Clin. Neurophysiol. *94*, 191–220.

Halgren, E., Baudena, P., Clarke, J.M., Heit, G., Marinkovic, K., Devaux, B., Vignal, J.P., and Biraben, A. (1995b). Intracerebral potentials to rare target and distractor auditory and visual stimuli: 2. Medial, lateral and posterior temporal lobe. Electroenceph. Clin. Neurophysiol. *94*, 229–250.

Hämäläinen, M.S., and Ilmoniemi, R.J. (1984). Interpreting measured magnetic fields of the brain: estimates of current distribution (Helsinki: University of Technology, Dept. of Technical Physics Report TKK-F-A559).

Hämäläinen, M.S., Hari, R., Ilmoniemi, R.J., Knuutila, J., and Lounasmaa, O.V. (1993). Magnetoencephalography—theory, instrumentation, and applications to noninvasive studies of the working human brain. Rev. Mod. Phys. *65*, 413–497.

Heinze, H.J., Mangun, G.R., Burchert, W., Hinrichs, H., Scholz, M., Munte, T.F., Gos, A., Scherg, M., Johannes, S., Hundeshagen, H., et al. (1994). Combined spatial and temporal imaging of brain activity during visual selective attention in humans. Nature *372*, 543–546.

Kutas, M., and Van Petten, C. (1988). Event-related brain potential studies of language. In Advances in Psychophysiology, P.K. Ackles, J.R. Jennings, and M.G.H. Coles, eds. (Greenwich, CT: JAI Press), pp. 139–187.

Kwong, K.K., Belliveau, J.W., Chesler, D.A., Goldberg, I.E., and Weisskoff, R.M. (1992). Dynamic magnetic resonance imaging of human brain activity during primary sensory stimulation. Proc. Nat. Acad. Sci. USA *89*, 5675–5679.

Liu, A.K. (2000). Spatiotemporal brain imaging. PhD dissertation, Massachusetts Institute of Technology, Cambridge, Massachusetts.

Liu, A.K., Belliveau, J.W., and Dale, A.M. (1998). Spatiotemporal imaging of human brain activity using fMRI constrained MEG data: Monte Carlo simulations. Proc. Nat. Acad. Sci. USA *95*, 8945–8950.

Mangun, G., Buonocore, M., Girelli, M., and Jha, A. (1998). ERP and fMRI measures of visual spatial selective attention. Hum. Brain Mapp. *6*, 383–389.

Martinez, A., Anllo-Vento, L., Sereno, M.I., Frank, L.R., Buxton, R.B., Dubowitz, D.J., Wong, E.C., Hinrichs, H., Heinze, H.J., and Hillyard, S.A. (1999). Involvement of striate and extrastriate visual cortical areas in spatial attention. Nat. Neurosci. *2*, 364–369.

Mazziotta, J.C., Phelps, M.E., and Halgren, E. (1983). Local cerebral glucose metabolic response to audiovisual stimulation and deprivation: studies in human subjects with positron CT. Hum. Neurobiol. *2*, 11–23.

McCarthy, G., Nobre, A.C., Bentin, S., and Spencer, D.D. (1995). Language-related field potentials in the anterior-medial temporal lobe: I. Intracranial distribution and neural generators. J. Neurosci. *15*, 1080–1089.

Menke, W. (1989). Geophysical Data Analysis: Discrete Inverse Theory (San Diego, CA: Academic Press).

Mesulam, M.M. (1990). Large-scale neurocognitive networks and distributed processing for attention, language, and memory. Ann. Neurol. *28*, 597–613.

Mitzdorf, U. (1985). Current source-density method and application in cat cerebral cortex: investigation of evoked potentials and EEG phenomena. Physiol. Rev. *65*, 37–100.

Mosher, J.C., Lewis, P.S., and Leahy, R.M. (1992). Multiple dipole modeling and localization from spatio-temporal MEG data. IEEE Trans. Biomed. Eng. *39*, 541–557.

Murray, E.A., and Bussey, T.J. (1999). Perceptual-mnemonic functions of the perirhinal cortex. Trends Cog. Sci. *3*, 142–151.

Nenov, V.I., Halgren, E., Smith, M.E., Badier, J.M., Ropchan, J.R., Blahd, W.H., and Mandelkern, M. (1991). Localized brain metabolic response correlated with potentials evoked by words. Behav. Brain Res. *44*, 101–104.

Nicholson, C., and Freeman, J.A. (1975). Theory of current source density analysis and determination of the conductivity tensor for anuran cerebellum. J. Neurophysiol. *38*, 356–368.

Nobre, A.C., and McCarthy, G. (1995). Language-related field potentials in the anterior-medial temporal lobe: II. Effects of word type and semantic priming. J. Neurosci. *15*, 1090–1098.

Nobre, A., Allison, T., and McCarthy, G. (1994). Word recognition in the human inferior temporal lobe. Nature *372*, 260–263.

Nunez, P.L. (1981). Electric Fields of the Brain (New York: Oxford University).

Oostendorp, T.F., and Van Oosterom, A. (1992). Source parameter estimation using realistic geometry in bioelectricity and biomagnetism. In Biomagnetic Localization and *3D Modeling*, J. Nenonen, H.M. Rajala, and T. Katila, eds. (Helsinki: Helsinki University of Technology, Report TKK-F-A689).

Picard, N., and Strick, P.L. (1996). Motor areas of the medial wall:

a review of their location and functional activation. Cereb. Cortex *6*, 342–353.

Portin, K., Salenius, S., Salmelin, R., and Hari, R. (1998). Activation of the human occipital and parietal cortex by pattern and luminance stimuli: neuromagnetic measurements. Cereb. Cortex *8*, 253–260.

Press, W.H., Teukolsky, S.A., Vetterling, W.T., and Flannery, B.P. (1994). Numerical Recipes in C, Second Edition (Cambridge: Cambridge University Press).

Prichard, J., Rothman, D., Novotny, E., Petroff, O., Kuwabara, T., Avison, M., Howseman, A., Hanstock, C., and Shulman, R. (1991). Lactate rise detected by 1H NMR in human visual cortex during physiologic stimulation. Proc. Natl. Acad. Sci. USA *88*, 5829–5831.

Puce, A., Allison, T., Spencer, S.S., Spencer, D.D., and McCarthy, G. (1997). Comparison of cortical activation evoked by faces measured by intracranial field potentials and functional MRI: two case studies. Hum. Brain Mapp. *5*, 298–305.

Raichle, M.E. (1987). Circulatory and metabolic correlates of brain function in normal humans. In Handbook of Physiology: The Nervous System V, Higher Functions of the Brain, F. Plum, ed. (Bethesda, MD: Amer. Physiol. Soc.), pp. 643–674.

Raichle, M.E., Fiez, J.A., Videen, T.O., MacLeod, A.-M.K., Pardo, J.V., Fox, P.T., and Petersen, S.E. (1994). Practice-related changes in human brain functional anatomy during nonmotor learning. Cereb. Cortex *4*, 8–26.

Reese, T.G., Davis, T.L., and Weisskoff, R.M. (1995). Automated shimming at 1.5 Tesla using echo planar image frequency maps. J. Magn. Reson. Imaging *5*, 739–745.

Regan, D. (1989). Human Brain Electrophysiology (New York: Elsevier).

Schmidt, D.M., George, J.S., and Wood, C.C. (1999). Bayesian inference applied to the electromagnetic inverse problem. Hum. Brain Mapp. *7*, 195–212.

Schroeder, C.E., Steinschneider, M., Javitt, D.C., Tenke, C.E., Givre, S.J., Mehta, A.D., Simpson, G.V., Arezzo, J.C., and Vaughan, H.G., Jr. (1995). Localization of ERP generators and identification of underlying neural processes. Electroencephalogr. Clin. Neurophysiol. Suppl. *44*, 55–75.

Sereno, M.I., Dale, A.M., Reppas, J.B., Kwong, K.K., Belliveau, J.W., Brady, T.L., Rosen, B.R., and Tootell, R.B.H. (1995). Borders of multiple visual areas in human revealed by functional magnetic resonance imaging. Science *268*, 889–893.

Sherg, M., and VonCramon, D. (1985). Two bilateral sources of the late AEP as identified by a spatio-temporal dipole model. Electroenceph. Clin. Neurophysiol. *62*, 32–44.

Shoham, D., Glaser, D.E., Arieli, A., Kenet, T., Wijnbergen, C., Toledo, Y., Hildesheim, R., and Grinvald, A. (1999). Imaging cortical dynamics at high spatial and temporal resolution with novel blue voltage-sensitive dyes. Neuron *24*, 791–802.

Smith, M.E., Stapleton, J.M., and Halgren, E. (1986). Human medial temporal lobe potentials evoked in memory and language tasks. Electroencephalogr. Clin. Neurophysiol. *63*, 145–159.

Snyder, A.Z., Abdullaev, Y.G., Posner, M.I., and Raichle, M.E. (1995). Scalp electrical potentials reflect regional cerebral blood flow responses during processing of written words. Proc. Nat. Acad. Sci. USA *92*, 1689–1693.

Sukov, W., and Barth, D.S. (1998). Three-dimensional analysis of spontaneous and thalamically evoked gamma oscillations in auditory cortex. J. Neurophysiol. *79*, 2875–2884.

Talairach, J., Szikla, G., Tournoux, P., Prossalentis, A., Bordas-Ferrer, M., Covello, L., Jaco, M., and Mempel, E. (1967). Atlas d'Anatomie Stereotaxique du Telencephale (Paris: Masson et Cie.).

Tsodyks, M., Kenet, T., Grinvald, A., and Arieli, A. (1999). Linking spontaneous activity of single cortical neurons and the underlying functional architecture. Science *286*, 1943–1946.

Ungerleider, L.G., and Mishkin, M. (1982). Two cortical visual systems. In Analysis of Visual Behavior, D.J. Ingle, M.A. Goodale, and R.J.W. Mansfield, eds. (Cambridge, MA: MIT press), pp. 549–586.

van Oosterom, A. (1999). The use of the spatial covariance in computing pericardial potentials. IEEE Trans. Biomed. Eng. *46*, 778–787.